nature portfolio

https://doi.org/10.1038/s41586-023-05730-4

Supplementary information

Determining the gluonic gravitational form factors of the proton

In the format provided by the
authors and unedited

Supplemental material

December 19, 2022

1 Definitions

The standard decomposition of the energy-momentum tensor is expressed in terms of the three gravitational form factors $A(K^2)$, $B(k^2)$, and $C(k^2)$.

$$\langle p_2|T^{\mu\nu}(0)|p_1\rangle = \bar{u}(p_2)\left(A(k)\gamma^{(\mu}p^{\nu)} + B(k)\frac{ip^{(\mu}p^{\nu)}k_\alpha}{2M} + C(k)\frac{k^\mu k^\nu - \eta^{\mu\nu}k^2}{M}\right)u(p_1) \quad (1)$$

The $C(k^2)$ form factor is typically called the $D(k^2)$ form factor in the framework of the Generalized Parton Distributions (GPDs) case where $D(k^2) = 4C(k^2)$. In the case separation of quarks and gluons is needed, this decomposition becomes for the quarks and gluons separately

$$\langle p_2|T^{\mu\nu}_{q,g}(0)|p_1\rangle = \bar{u}(p_2)\left(A_{q,g}(k)\gamma^{(\mu}p^{\nu)} + B_{q,g}(k)\frac{ip^{(\mu}p^{\nu)}k_\alpha}{2M} + C_{q,g}(k)\frac{k^\mu k^\nu - \eta^{\mu\nu}k^2}{M} + \bar{C}_{q,g}(k^2)g^{\mu\nu}M\right)u(p_1) \quad (2)$$

with the relations

$$A_q(k^2) + A_g(k^2) = A(k^2) \quad (3)$$
$$B_q(k^2) + B_g(k^2) = B(k^2) \quad (4)$$
$$C_q(k^2) + C_g(k^2) = C(k^2) \quad (5)$$
$$\bar{C}_q(k^2) + \bar{C}_g(k^2) = 0 \quad (6)$$

2 Formulas used in the 2D fit

In our extraction of the $A_g(k^2)$ and $C_g(k^2)$ gravitational form factors we used two different approaches found in the literature: One dubbed holographic QCD approach [1, 2] the other the GPD approach [3]. In the holographic QCD approach, early publications only considered $A_g(k^2)$, neglecting $C_g(k^2)$ in the expression of the cross section. The more recent work in Ref. [4] used both $A_g(k^2)$ and $C_g(k^2)$ in the expression for the differential cross-section. This approach enabled us to extract the m_A coefficient of the tripole form of $A_g(k^2)$ and both $C_g(0)$ and m_C of the tripole form of the $C_g(k^2)$ gluonic form factor simultaneously.

2.1 Holographic QCD

In the case of the holographic QCD approach, we used formula (III.31) on page 9 in Ref. [4]. Furthermore, we fixed $A_g(0)$ to the average gluon PDF from CT18 [5]. The remaining three parameters $C_g(0)$, m_A and m_C were left as free parameters and fit simultaneously to our cross section results. We took the normalization constant $\mathcal{N} \cdot e = 7.768(\mathrm{nb/GeV}^6)^{1/2}$ from Ref. [1], where the authors constrained this value based on the 2019 GlueX cross section results [6]. The expression of the differential cross section we used is given by;

$$\frac{d\sigma}{dt} = \mathcal{N}^2\frac{e^2}{(W^2 - M_N^2)^2}\frac{A_g^2(t) + 8\eta^2 A_g(t)C_g(t) + 16\eta^4 C_g(t)}{4A_g^2(0)}F(s,t,M_V,M_N)\left(\frac{-2t}{M_N^2} + 8\right) \quad (7)$$

where M_N is the mass of the nucleon, M_V is the mass of vector meson, W is the invariant mass of the photon-nucleon system ($W = \sqrt{(s)}$ where s is the Mandelstam variable), and t is the Mandelstam variable

- square of momentum transferred from the initial photon to the produced vector meson. The kinematical function $F(s,t,M_V,M_N)$ is taken from equation 8.6 from Ref. [1]. The skewness parameter, η defined in reference [4] equation (III.33), follows the definition from [7]:

$$\eta = \frac{M_V^2}{4p_1\cdot q - M_V^2 + t} \tag{8}$$

where $2p_1.q = s - M_N^2 = W^2 - M_N^2$.

2.2 Generalized Parton Distributions

In the case of the GPD approach, we used equations (17) and (26), (38), and (39) of ref. [3]. Here also we fix $A_g(0)=\langle x\rangle_g$ using CT18 pdfs [5] and we treat $C(0)$, m_A and m_C. The cross section expression is given by,

$$\frac{d\sigma}{dt} = \frac{\alpha_{EM}e_Q^2}{4(W^2-M_N^2)^2}\frac{(16\pi\alpha_S)^2}{3M_V^3}|\psi_{NR}(0)|^2|G(t,\xi)|^2, \tag{9}$$

where,

$$|G(t,\xi)|^2 = \frac{1}{\xi^4}\left\{\left(1-\frac{t}{4M_N^2}\right)E_2^2 - 2E_2(E_2+H_2) + (1-\xi^2)(H_2+E_2)^2\right\}, \tag{10}$$

and,

$$H_2 = A_{2,0g}(t) + (2\xi)^2 C_{2g} \tag{11}$$

$$E_2 = B_{2,0g}(t) - (2\xi)^2 C_{2g} \tag{12}$$

Following the approach of Ref.[3], we used $\alpha_S = 0.3$ and the non-relativistic wavefunction $|\psi_{NR}(0)|^2 = 1.0952/(4\pi)$ GeV^3 (which was calculated from the leptonic decay rate of J/ψ). M_N and M_V are the nucleon's and charmonium's mass, respectively. e_Q is the charge of quarks (=2/3) in units of proton charge. ξ is the skewness parameter defined as

$$\xi = \frac{P^+ - P'^+}{P^+ + P'^+} \tag{13}$$

where P and P' are the incoming and outgoing proton momenta in the c.m frame. The superscript + is denoting the light-front coordinate defined as $x^+ = (x^0 + x^z)/\sqrt{2}$
We used a tripole ansatz for $A_g(t)$ and $C_g(t)$:

$$A_g(t) = \frac{A_g(0)}{\left(1-\frac{t}{m_A^2}\right)^3}, \qquad C_g(t) = \frac{C_g(0)}{\left(1-\frac{t}{m_C^2}\right)^3} \tag{14}$$

3 Impact of the high t data on the results

To explore the impact of our large t data at values beyond those that were published by GlueX in 2019 [6], we compared the results of a fit to our full data set to a fit restricted to only those data points where $|t| < 1.4$ GeV^2. For this comparison, we used a dipole functional form of the one dominant form factor $A(t)$ and determined the scale parameter m_A of equation (15). The full data set results are shown in the top panel of Fig. 1, where the parameter m_A is reported in Table 1. We then repeated the fit ignoring data when $t > 1.4$ GeV^2, and the results are shown in the bottom panel of Fig. 1 and Table 2. Comparing the top and bottom panels, we get an idea of the impact of the large t data to constrain the functional form and allow a more accurate extrapolation to the forward limit ($t = 0$). Without the strong lever-arm provided by the high-t data the data are not able to fully constrain the dipole slope in the lower energy bins, and in all cases, the error on the fit parameters and derived quantities is much larger when only considering data at low t.

3.1 Dipole fit for each photon energy bin

$$\frac{d\sigma}{dt} = \left.\frac{d\sigma}{dt}\right|_{t=0}\frac{1}{(1-t/m_A^2)^4} \tag{15}$$

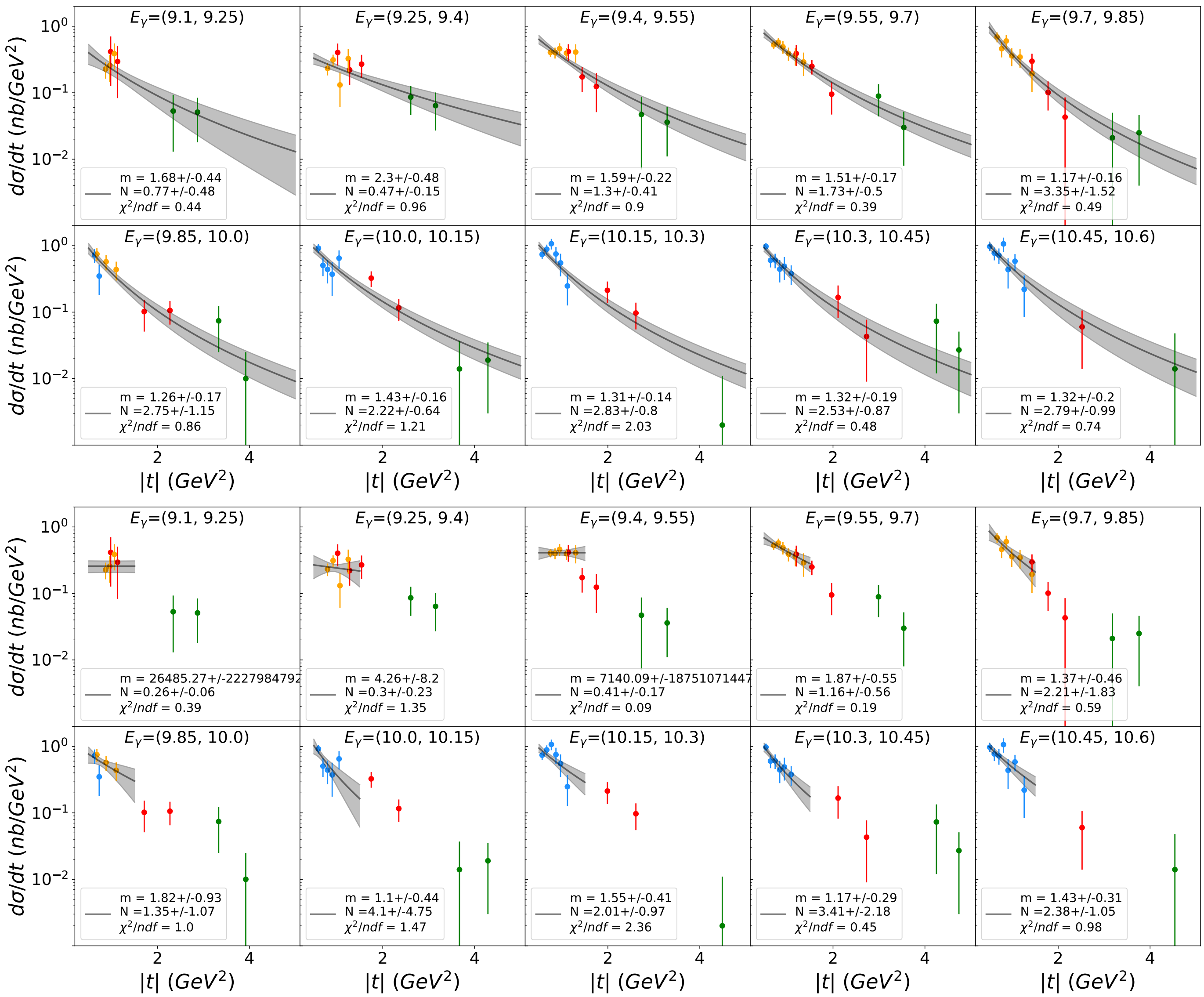

Figure 1: Top panels: Dipole fit to the differential cross section $d\sigma/dt$ using the full data set. Bottom panels: only for data when when $|t| < 1.41\ GeV^2$. At each energy the insert indicates m_A labeled as m and the differential cross section at $t = 0$ as N. The coefficients are summarized in Tables 1 & 2.

3.2 Exponential fits for each photon energy bin

The added points at high t are important to constrain the exact functional form of the t-dependence in the first place. To illustrate, we compare the dipole shape from the previous subsection, motivated by the physics of two gluon exchange, with an exponential ansatz. The exponential functional form is as follows:

$$\frac{d\sigma}{dt} = \left.\frac{d\sigma}{dt}\right|_{t=0} \exp(-2b'|t|) = \left.\frac{d\sigma}{dt}\right|_{t=0} \exp(-b|t|) \tag{16}$$

Comparing the fit procedure using either ansatz gives consistent results between both functional forms, as shown by comparing the top panels of Fig 1 and 2 and the fit results in Tables 1 and 3. In contrast, if one truncates our data set to the region in t published by GlueX at each photon energy, we see that the different model ansatzes for the functional shape give drastically different results, as shown by comparing the bottom panels of Fig 1 and 2 and the fit results in Tables 2 and 4. This is particularly the case at

E_{bin} (GeV)	m_A (GeV)	$d\sigma/dt\|_{t=0}$ nb/GeV^2	$\chi^2/n.d.f$
9.10-9.25	1.68 ± 0.44	0.77 ± 0.48	0.44
9.25-9.40	2.3 ± 0.48	0.47 ± 0.15	0.96
9.40-9.55	1.59 ± 0.22	1.3 ± 0.41	0.9
9.55-9.70	1.51 ± 0.17	1.73 ± 0.5	0.39
9.70-9.85	1.17 ± 0.16	3.35 ± 1.52	0.49
9.85-10.00	1.26 ± 0.17	2.75 ± 1.15	0.86
10.00-10.15	1.43 ± 0.16	2.22 ± 0.64	1.21
10.15-10.30	1.31 ± 0.14	2.83 ± 0.8	2.03
10.30-10.45	1.32 ± 0.19	2.53 ± 0.87	0.48
10.45-10.60	1.32 ± 0.2	2.79 ± 0.99	0.74

Table 1: Parameters of the dipole fit to the differential cross section $d\sigma/dt$ using all data sets. Fits shown in Figure 1 top panel

E_{bin} (GeV)	m_A (GeV)	$d\sigma/dt\|_{t=0}$ nb/GeV^2	$\chi^2/n.d.f$
9.10-9.25	26485.27 ± 222798479286.07	0.26 ± 0.06	0.39
9.25-9.4	4.26 ± 8.2	0.3 ± 0.23	1.35
9.40-9.55	7140.09 ± 18751071447.65	0.41 ± 0.17	0.09
9.55-9.70	1.87 ± 0.55	1.16 ± 0.56	0.19
9.70-9.85	1.37 ± 0.46	2.21 ± 1.83	0.59
9.85-10.00	1.82 ± 0.93	1.35 ± 1.07	1.0
10.00-10.15	1.1 ± 0.44	4.1 ± 4.75	1.47
10.15-10.30	1.55 ± 0.41	2.01 ± 0.97	2.36
10.30-10.45	1.17 ± 0.29	3.41 ± 2.18	0.45
10.45-10.6	1.43 ± 0.31	2.38 ± 1.05	0.98

Table 2: Dipole fit to the differential cross section $d\sigma/dt$ for $|t| < 1.41\ GeV^2$. Fit shown in Figure 1 bottom panel.

lower photon energies. In the lowest energy bin, the exponential shape is so poorly constrained that the slope versus $|t|$ rises instead of the usual falling slope. Therefore we are of the opinion that the large t data is important to constrain the t dependence on the form factors. In fact, when going to the 2-D combined fits the physics-driven dipole (or tripole) shapes required for the M-Z, and G-J-L approaches are strongly favored versus the linear-like exponential ansatz. This distinction is fully driven by the need to describe all high-t data simultaneously.

4 G-J-L GPD approach fit to GlueX

In this section, we investigate the impact of the $J/\psi - 007$ results compared to what could be accomplished with the 2019 GlueX results [6].

First, to validate our extraction procedure, we performed a similar two-parameter fit as described in the G-J-L GPD approach to the GlueX data. The results are shown in Figure 3. In this procedure the differential cross section and the total cross section are fitted simultaneously with two fixed parameters $A_g(0) = 0.58$ and $m_C = 0.48$. While these values are known not to be optimal (in particular, this value for $A_g(0)$ is inconsistent with recent PDF parametrizations), we followed the approach as written to benchmark our fit procedure. Our fit results were $m_A = 1.67 \pm 0.13$ and $C_g(0) = -0.77 \pm 0.96$, while G-J-L reported $m_A = 1.64 \pm 0.11$ and $C_g(0) = -0.84 \pm 0.82$ in their paper. We clarified this difference with the authors and found that this was due to a small misprint in the value of α_e electromagnetic in their extraction routines (they used $\alpha_e = 1/133$ instead of $\alpha_e = 1/137$). Otherwise, we find the exact same results as in [3].

Following this validation step, we repeated the analysis with the GlueX data but choosing a more realistic $A_g(0)$=0.41[1] and $m_C = 1.07$ (GeV) from the most recent lattice QCD calculations. We then repeated the

[1]This value is consistent with all recent PDF parametrizations for the gluon PDF.

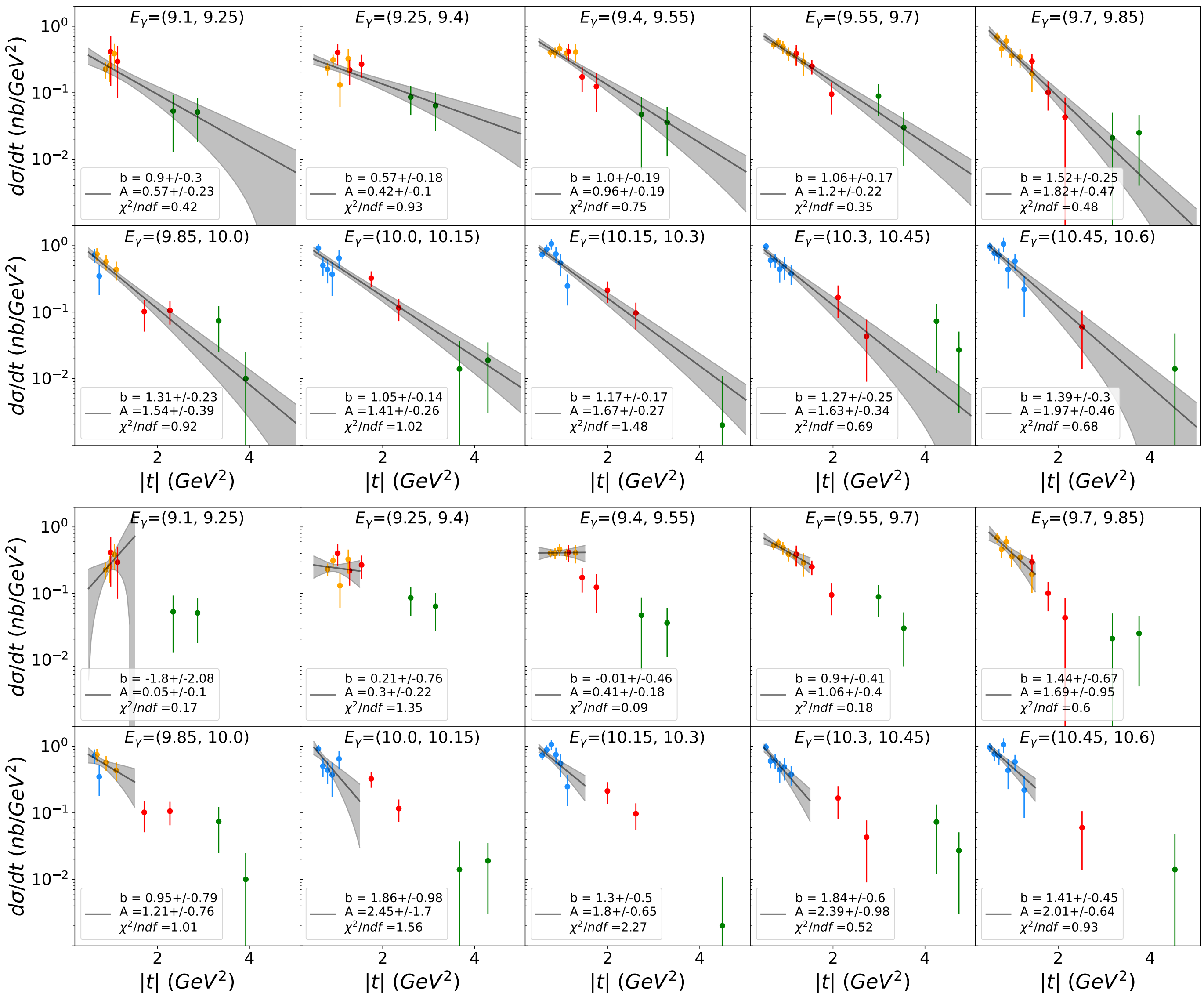

Figure 2: Top panels: Exponential fit to the differential cross section $d\sigma/dt$ using the full data set. Bottom panels: only for data when when $|t| < 1.41$ GeV^2. At each energy the insert indicates b and the differential cross section at $t = 0$ labeled as A N. The coefficients are summarized in Table 3 & 4.

fit to extract $C_g(0)$ and m_A to explore the impact of GlueX compared to the $J/\psi - 007$ experiment. The result of this fit is represented by the grey band in Fig.4, where it is compared with the results of the full 3-parameter tripole fit to the J/ψ-007 data set. Note that for this comparison $A_g(0)$ was fixed consistently between both extractions, and m_C was set to a lattice result that is very close to the result from the $J/\psi-007$ experiment. We observe that even in this case, and ignoring the added model uncertainty for a 2-parameter extraction versus a free 3-parameter fit, the GlueX data alone are insufficient to constrain even the sign of the D form factor.

E_{bin} (GeV)	b (GeV^{-2})	$d\sigma/dt\|_{t=0}$ nb/GeV^2	$\chi^2/n.d.f$
9.10-9.25	0.9 ± 0.3	0.57 ± 0.23	0.42
9.25-9.40	0.57 ± 0.18	0.42 ± 0.1	0.93
9.40-9.55	1.0 ± 0.19	0.96 ± 0.19	0.75
9.55-9.70	1.06 ± 0.17	1.2 ± 0.22	0.35
9.70-9.85	1.52 ± 0.25	1.82 ± 0.47	0.48
9.85-10.00	1.31 ± 0.23	1.54 ± 0.39	0.92
10.00-10.15	1.05 ± 0.14	1.41 ± 0.26	1.02
10.15-10.30	1.17 ± 0.17	1.67 ± 0.27	1.48
10.30-10.45	1.27 ± 0.25	1.63 ± 0.34	0.69
10.45-10.60	1.39 ± 0.3	1.97 ± 0.46	0.68

Table 3: Exponential fit to the differential cross section $d\sigma/dt$ using all the data set. Fits shown in Figure 2 top panel.

E_{bin} (GeV)	b (GeV^{-2})	$d\sigma/dt\|_{t=0}$ nb/GeV^2	$\chi^2/n.d.f$
9.10-9.25	-1.8 ± 2.08	0.05 ± 0.1	0.17
9.25-9.40	0.21 ± 0.76	0.3 ± 0.22	1.35
9.40-9.55	-0.01 ± 0.46	0.41 ± 0.18	0.09
9.55-9.70	0.9 ± 0.41	1.06 ± 0.4	0.18
9.70-9.85	1.44 ± 0.67	1.69 ± 0.95	0.6
9.85-10.00	0.95 ± 0.79	1.21 ± 0.76	1.01
10.00-10.15	1.86 ± 0.98	2.45 ± 1.7	1.56
10.15-10.30	1.3 ± 0.5	1.8 ± 0.65	2.27
10.30-10.45	1.84 ± 0.6	2.39 ± 0.98	0.52
10.45-10.60	1.41 ± 0.45	2.01 ± 0.64	0.93

Table 4: Exponential fit to differential cross section $d\sigma/dt$ for $|t| < 1.41\ GeV^2$. Fit shown in Figure 2 bottom panel.

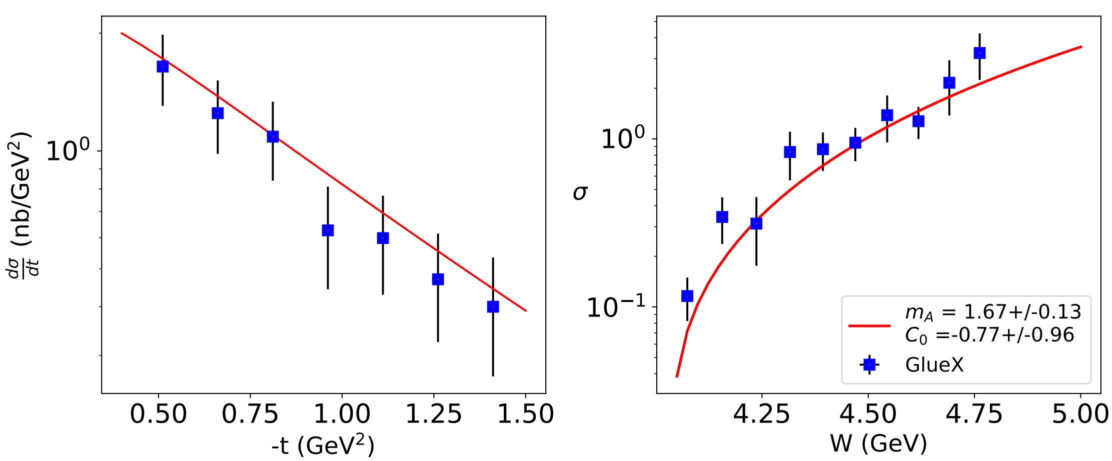

Figure 3: Fit to the GlueX data following the GPD approach of G-J-L with both $A_g(0) = 0.58$ and $m_C = 0.48$ fixed on lattice QCD. The results from this fit lead to the $A(k^2)$ and the $C(k)$ represented in a grey band.

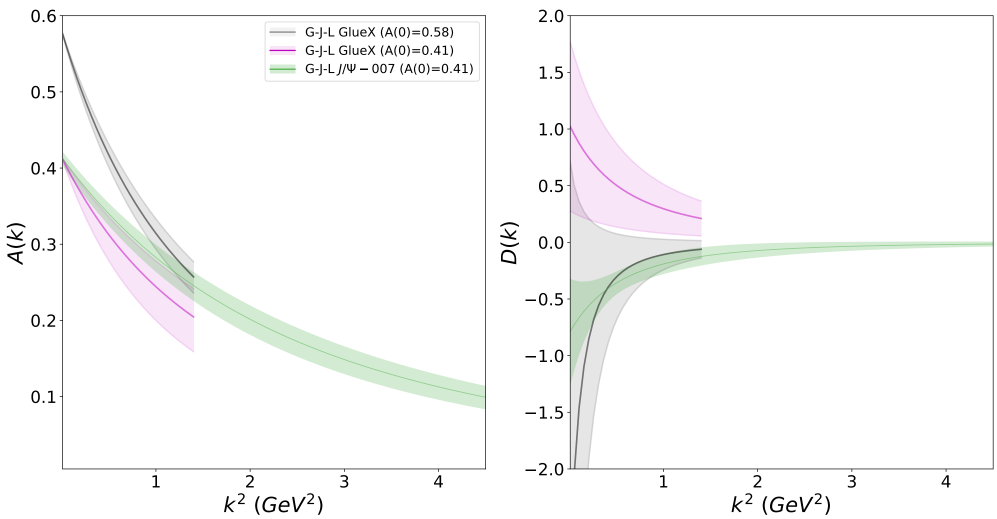

Figure 4: $A_g(k^2)$ and $D_g(k^2)$ dipole form factors from the extracted parameters using G-J-L approach. Pink and grey curves show the form factors extracted from GlueX data with A(0) equal to 0.58 and 0.41, respectively. The green curves show the tripole form factors extracted from the analysis of $J/\psi - 007$ data.

5 J/ψ-007 2D fits

The quality of the 2D fits performed using the full data set to extract $A_g(k^2)$ and $C(\mathrm{k}^2)$ in the M-Z and GPD approaches is shown in Figs. 6 and 7, respectively

5.1 M-Z or holographic QCD approach

As an example, in Fig. 5, we show the 2D fit surface resulting from our fit. While in Fig. 6 we display the result by photon energy bin.

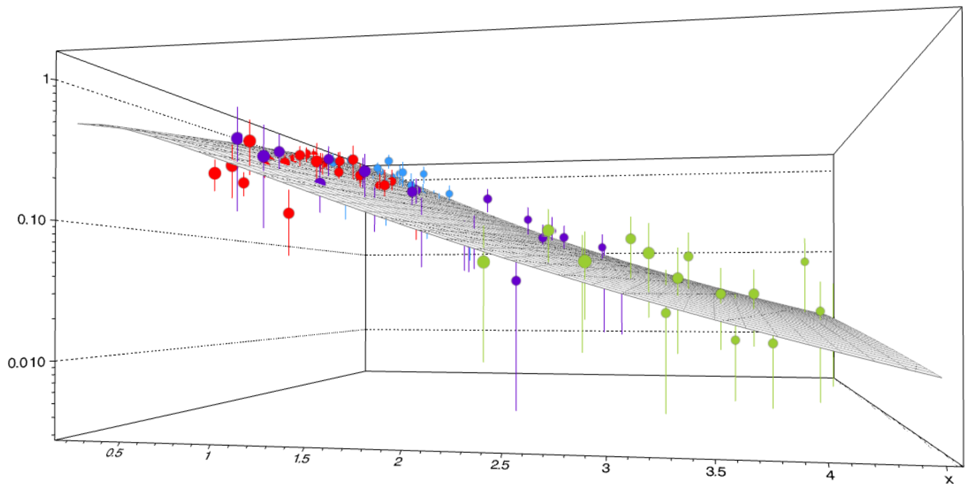

Figure 5: 2D fit to $d\sigma/dt$ data of J/ψ-007 experiment using the M-Z approach. Note that taken together the large t data are important to provide a constraint on the form factors

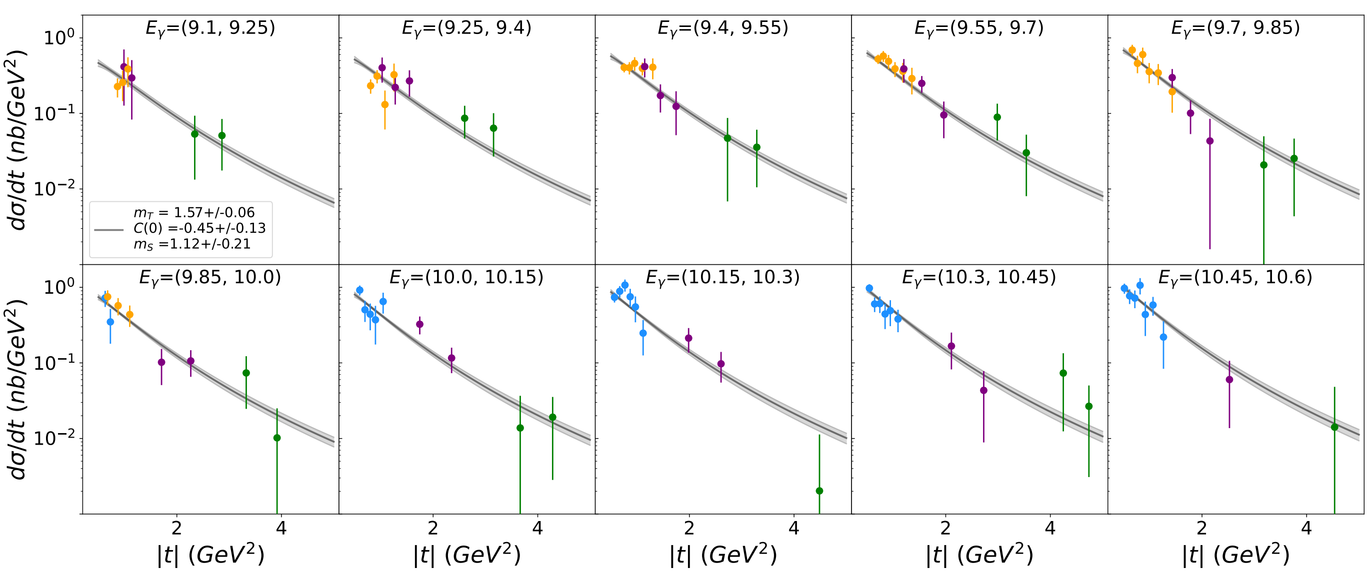

Figure 6: 2D fit to J/ψ-007 $d\sigma/dt$ using M-Z approach and displayed in separate energy bins of equal size.

5.2 G-J-L or Generalized Parton Distributions approach

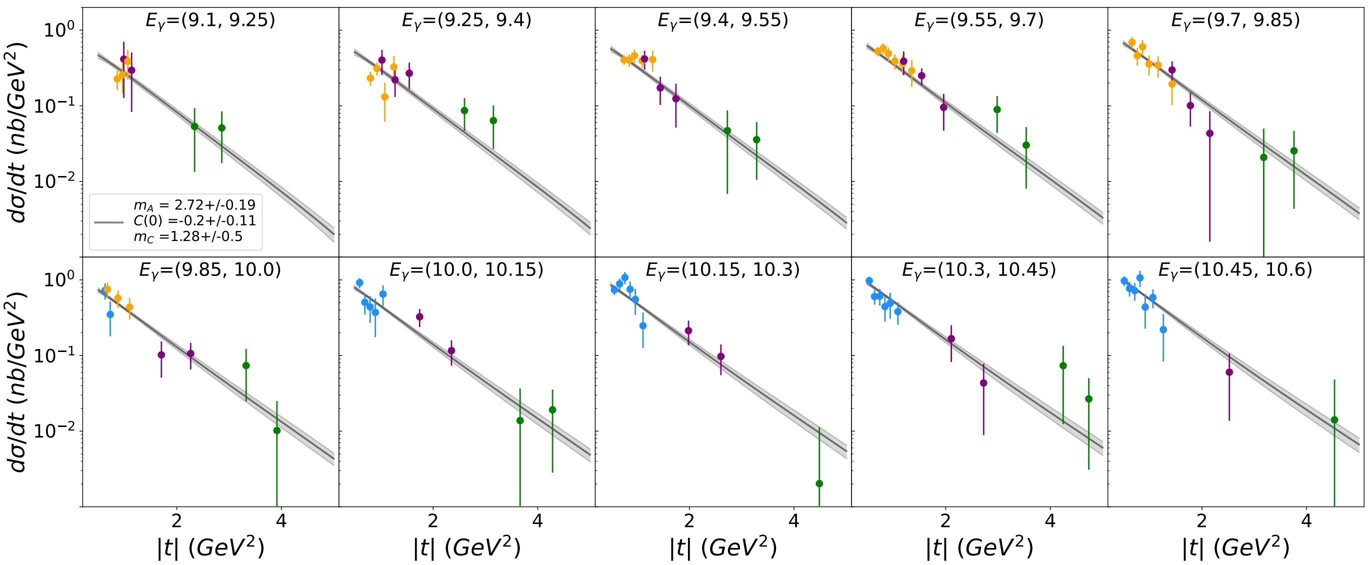

Figure 7: 2D fit to J/ψ-007 $d\sigma/dt$ using G-J-L approach

5.3 Model predictions with error bands

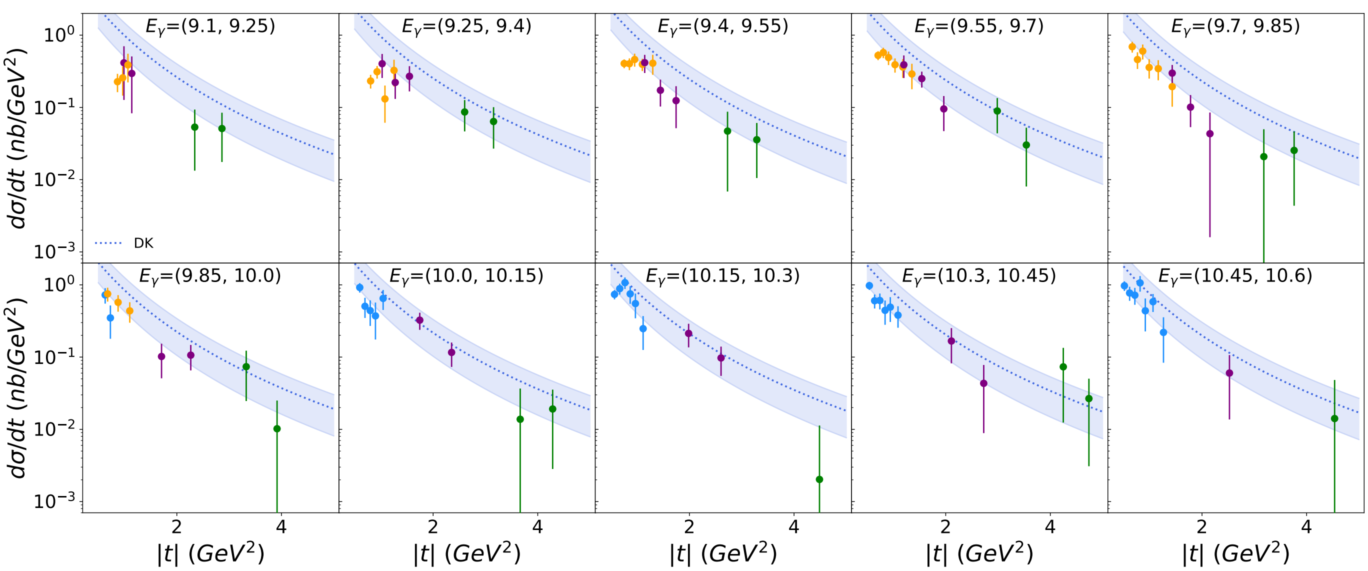

Figure 8: DK model prediction

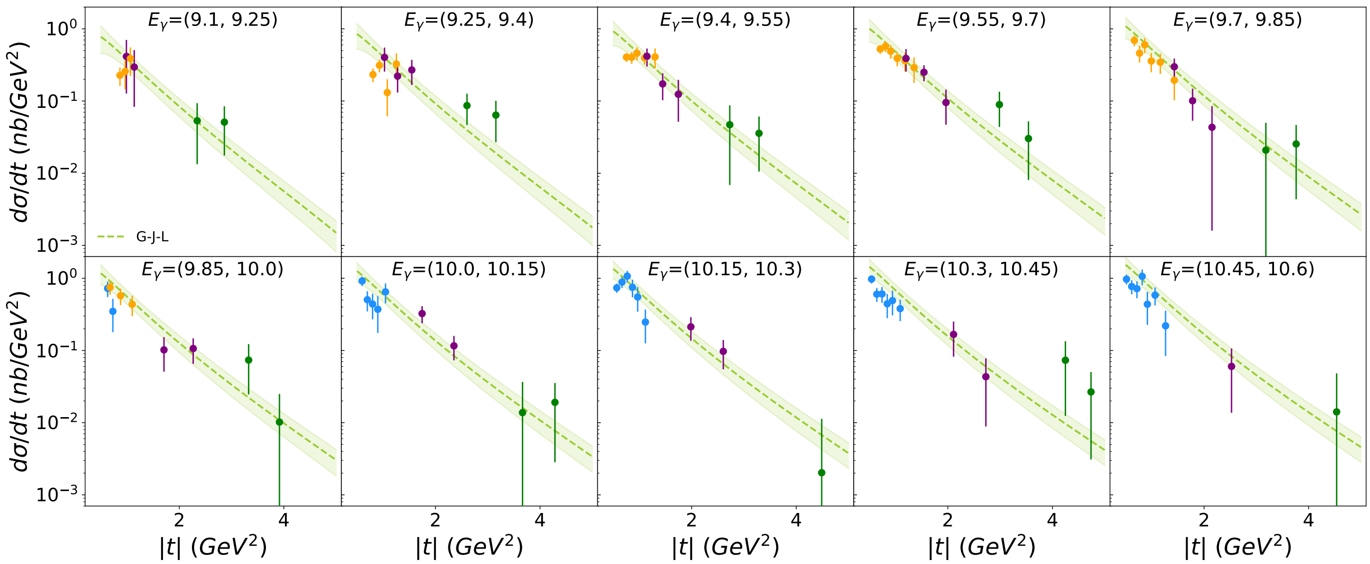

Figure 9: G-J-L model prediction

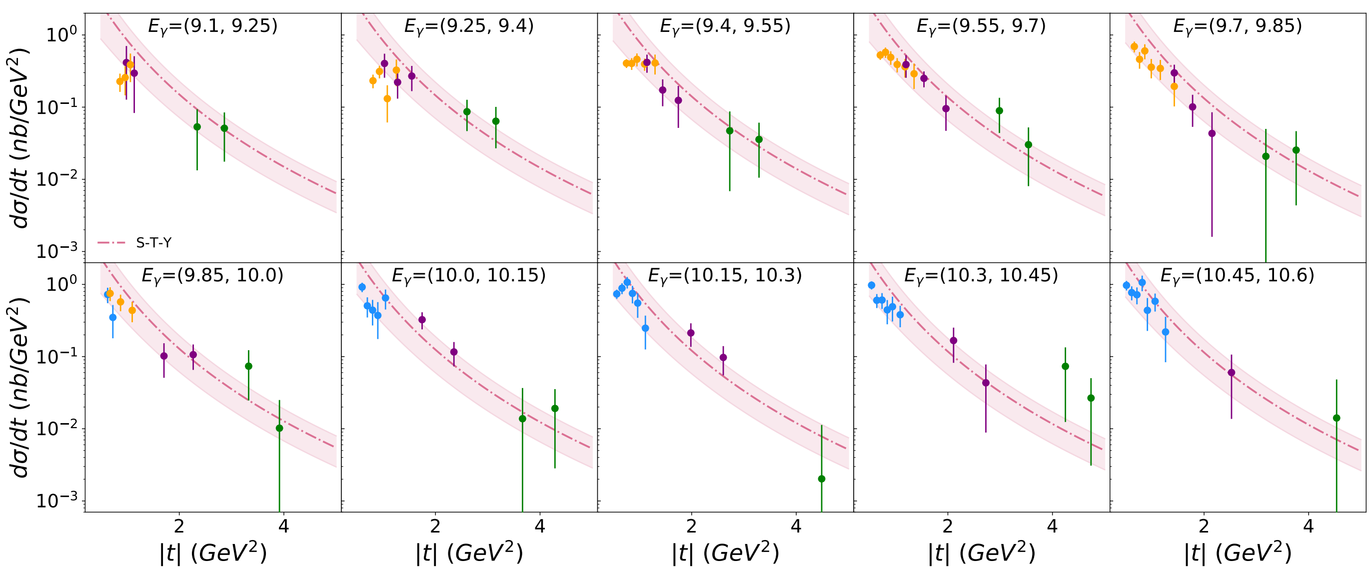

Figure 10: S-T-Y model prediction

6 Inelastic J/ψ Production

The general relation to constrain the photon energy for a $\gamma + p \to J/\psi + X$ reaction assuming a proton target at rest and a photon colinear with the z-axis is

$$E = \frac{1}{2}\frac{2M_pE_\psi + M_X^2 - M_p^2 - M_\psi^2}{M_p + P_\psi \cos\theta_\psi - E_\psi}, \tag{17}$$

which in case of elastic production (X is the recoil proton) reduces to

$$E_{\rm rec} = \frac{1}{2}\frac{2M_pE_\psi - M_\psi^2}{M_p + P_\psi \cos\theta_\psi - E_\psi}, \tag{18}$$

Assuming elastic J/ψ production while inelastic production (such as $\gamma + p \to J/\psi + p + \pi^0$) leads in all cases to lower reconstructed energy versus the true energy. Hence, the lower-energy data points are most sensitive to this background. At the same time, this background cannot impact the highest energy bins as the kinematic migration to this energy value would require photon energies beyond the available beam energy. During the proposal, we estimated the background based on the available higher energy data, where the inelastic cross section is about 30% of the elastic cross section. However, this ratio is expected to be much lower near the threshold due to the phase space closing. We expected our experimental setting 2 to be the most sensitive to this background, while the high-energy setting one should be mostly unaffected by this background.

We simulated this process for all detector settings to quantify the impact of the inelastic J/ψ production channel. For example, Fig. 11 shows the observed shift in reconstructed versus true photon energy and reconstructed versus true $|t|$ for setting 2. The energy shift is about 0.7 GeV, similar to all four experimental settings. Note that this energy shift makes it kinematically impossible to have inelastic background contamination in setting 1, as its energy acceptance of 9.85-10.6 GeV sits against the incident beam energy of 10.6 GeV. Hence, in this case, there is not enough energy available for inelastic J/ψ events that end up in the detector acceptance.

Furthermore, the large $|t|$-shift to lower values in Fig 11 predicts as signature for the inelastic events that we would reconstruct events below the allowed $t_{\min}$ for elastic J/ψ production. Moreover, this contribution should be the most significant contamination region, as the inelastic J/ψ production shows a rapidly falling behavior versus $|t|$, similar to elastic production. Fig. 12 shows the measured phase space for setting 2. There is no evidence for a significant background contribution in the number of J/ψ events reconstructed below $|t_{\min}|$.

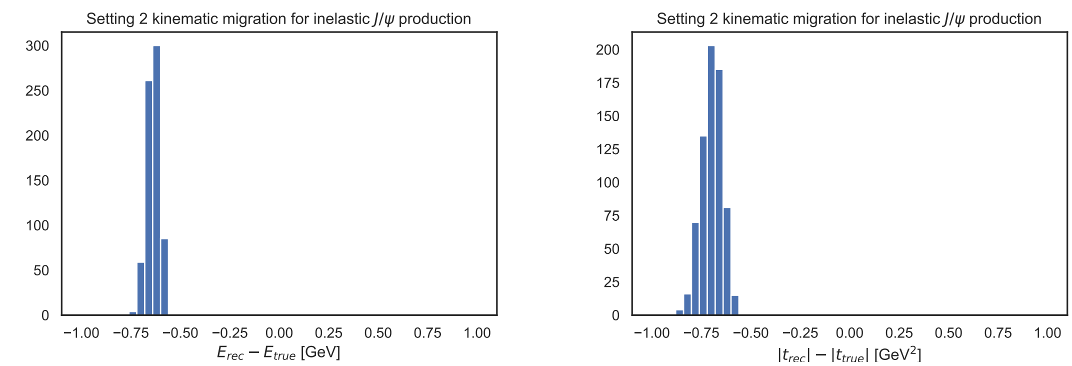

Figure 11: Left: Reconstructed energy minus true energy for inelastic J/ψ production in setting 2. Within the detector acceptance, the reconstructed energy is about 0.7 GeV lower than the true energy. Right: Same difference for Reconstructed minus true $|t|$. Here we see a shift of -0.75 GeV^2.

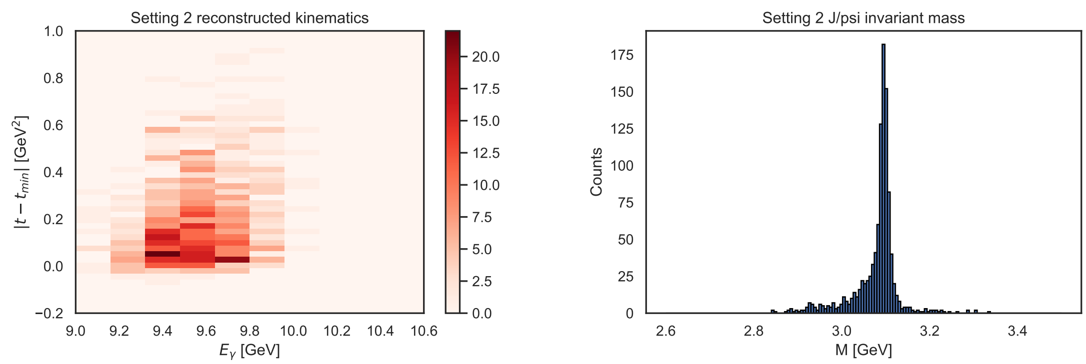

Figure 12: Left: Measured phase space in $|t - t_{\rm min}|$ versus E_γ for identified J/ψ events in setting 2. The color scale shows raw counts. Note the lack of events below zero (where $|t| < |t_{\rm min}|$). Right: Corresponding invariant mass histogram (before combinatoric background subtraction).

7 Cross Section Data

Table 5: Experimental differential cross sections results at different photon energies as a function of the four-momentum transfer t. The different labels in the columns correspond to the following. S is the setting number, idx is the index of this measurement within the setting S, E_{idx} is a photon energy bin index, t_idx is a $|t-t_{min}|$ bin index within this photon energy bin, E_{low} is the lower boundary of the photon energy bin, E_{high} is the upper boundary of the photon energy bin, Δt_l is the lower boundary of the $|t-t_{min-low}|$ bin, Δt_h is the upper boundary of the $|t-t_{min-high}|$ bin, E_{avg} is the average photon energy within the bin in GeV, Δt_{avg} is the average value of $t-t_{min}$ in this bin in GeV^2, $|t|_{avg}$ is the average value of $|t|$ in this bin (GeV^2), $d\sigma/dt$ is the cross section result in (nb/GeV^2), $\pm stat$ is the statistical uncertainty on the cross section result, $\pm sys$ is the systematic uncertainty and $\pm tot$ is the total uncertainty evaluated by adding in quadrature both statistical and the systematic uncertainty including a 4% scale uncertainty all in (nb/GeV^2). This table shows the results for setting 1.

S	idx	$E_{\rm idx}$	$t_{\rm idx}$	$E_{\rm low}$ (GeV)	$E_{\rm high}$ (GeV)	$\Delta t_{\rm low}$ (GeV^2)	$\Delta t_{\rm high}$ (GeV^2)	$E_{\rm avg}$ (GeV)	$\Delta t_{\rm avg}$ (GeV^2)	$\|t\|_{\rm avg}$ (GeV^2)	$d\sigma/dt$ (nb/GeV^2)	± stat	± sys	± tot
1	0	8	0	9.85	10	0	0.1	9.92	0.05	0.63	0.724	0.167	0.051	0.175
1	1	8	1	9.85	10	0.1	0.2	9.93	0.15	0.73	0.349	0.162	0.050	0.169
1	2	9	0	10	10.15	0	0.1	10.08	0.05	0.60	0.918	0.136	0.014	0.137
1	2	9	1	10	10.15	0.1	0.2	10.08	0.15	0.70	0.505	0.155	0.024	0.157
1	4	9	2	10	10.15	0.2	0.3	10.08	0.25	0.80	0.440	0.17	0.006	0.17
1	5	9	3	10	10.15	0.3	0.4	10.08	0.35	0.90	0.372	0.192	0.044	0.197
1	6	9	4	10	10.15	0.4	0.6	10.07	0.5	1.05	0.649	0.189	0.066	0.2
1	7	10	0	10.15	10.3	0.0	0.1	10.23	0.05	0.57	0.738	0.108	0.002	0.108
1	8	10	1	10.15	10.3	0.1	0.2	10.23	0.15	0.67	0.885	0.15	0.023	0.152
1	9	10	2	10.15	10.3	0.2	0.3	10.23	0.25	0.77	1.071	0.194	0.021	0.195
1	10	10	3	10.15	10.3	0.3	0.4	10.23	0.35	0.87	0.75	0.200	0.044	0.205
1	11	10	4	10.15	10.3	0.4	0.5	10.22	0.45	0.97	0.551	0.204	0.028	0.206
1	12	10	5	10.15	10.3	0.5	0.7	10.23	0.60	1.12	0.248	0.121	0.012	0.122
1	13	11	0	10.3	10.45	0.0	0.1	10.38	0.05	0.54	0.975	0.120	0.034	0.125
1	14	11	1	10.3	10.45	0.1	0.2	10.38	0.15	0.64	0.602	0.128	0.033	0.132
1	15	11	2	10.3	10.45	0.2	0.3	10.38	0.25	0.74	0.607	0.150	0.010	0.15
1	16	11	3	10.3	10.45	0.3	0.4	10.38	0.35	0.84	0.443	0.158	0.043	0.163
1	17	11	4	10.3	10.45	0.4	0.5	10.38	0.45	0.94	0.491	0.183	0.025	0.185
1	18	11	5	10.3	10.45	0.5	0.7	10.38	0.6	1.09	0.380	0.124	0.019	0.125
1	19	12	0	10.45	10.6	0.0	0.1	10.56	0.05	0.51	0.971	0.144	0.035	0.148
1	20	12	1	10.45	10.6	0.1	0.2	10.56	0.15	0.61	0.77	0.164	0.043	0.169
1	21	12	2	10.45	10.6	0.2	0.3	10.55	0.25	0.71	0.719	0.188	0.022	0.189
1	22	12	3	10.45	10.6	0.3	0.4	10.55	0.35	0.81	1.064	0.244	0.088	0.259
1	23	12	4	10.45	10.6	0.4	0.5	10.55	0.45	0.91	0.437	0.206	0.043	0.21
1	24	12	5	10.45	10.6	0.5	0.7	10.55	0.6	1.06	0.584	0.161	0.027	0.163
1	25	12	6	10.45	10.6	0.7	0.9	10.54	0.8	1.26	0.220	0.131	0.038	0.136

Table 6: Same as Table 5 for Setting 2.

S	idx	$E_{\rm idx}$	$t_{\rm idx}$	$E_{\rm low}$ (GeV)	$E_{\rm high}$ (GeV)	$\Delta t_{\rm low}$ (GeV^2)	$\Delta t_{\rm high}$ (GeV^2)	$E_{\rm avg}$ (GeV)	$\Delta t_{\rm avg}$ (GeV^2)	$\|t\|_{\rm avg}$ (GeV^2)	$d\sigma/dt$ (nb/GeV^2)	± stat	± sys	± tot
2	0	3	0	9.1	9.25	0.0	0.1	9.17	0.05	0.87	0.227	0.061	0.020	0.064
2	1	3	1	9.1	9.25	0.1	0.2	9.18	0.15	0.96	0.257	0.111	0.010	0.165
2	3	4	0	9.25	9.4	0.0	0.1	9.33	0.05	0.8	0.232	0.047	0.017	0.05
2	4	4	1	9.25	9.4	0.1	0.25	9.33	0.17	0.92	0.312	0.061	0.012	0.062
2	5	4	2	9.25	9.4	0.25	0.4	9.33	0.32	1.07	0.131	0.069	0.011	0.07
2	6	4	3	9.25	9.4	0.4	0.6	9.33	0.5	1.25	0.326	0.128	0.030	0.131
2	7	5	0	9.4	9.55	0.0	0.1	9.48	0.05	0.75	0.405	0.056	0.009	0.056
2	8	5	1	9.4	9.55	0.1	0.2	9.48	0.15	0.85	0.402	0.075	0.004	0.075
2	9	5	2	9.4	9.55	0.2	0.3	9.48	0.25	0.95	0.460	0.092	0.019	0.094
2	10	5	3	9.4	9.55	0.3	0.5	9.48	0.0	1.1	0.395	0.073	0.022	0.076
2	11	5	4	9.4	9.55	0.5	0.7	9.48	0.60	1.3	0.409	0.119	0.042	0.126
2	12	6	0	9.55	9.7	0.0	0.1	9.63	0.05	0.71	0.525	0.073	0.009	0.074
2	13	6	1	9.55	9.7	0.1	0.2	9.63	0.15	0.81	0.575	0.093	0.013	0.094
2	14	6	2	9.55	9.7	0.2	0.3	9.63	0.25	0.91	0.49	0.100	0.028	0.104
2	15	6	3	9.55	9.7	0.3	0.45	9.63	0.37	1.03	0.39	0.084	0.025	0.087
2	16	6	4	9.55	9.7	0.45	0.6	9.63	0.52	1.18	0.361	0.104	0.013	0.105
2	17	6	5	9.55	9.7	0.6	0.8	9.63	0.7	1.36	0.290	0.110	0.018	0.112
2	18	7	0	9.7	9.85	0.0	0.1	9.78	0.05	0.67	0.691	0.114	0.030	0.118
2	19	7	1	9.7	9.85	0.1	0.2	9.78	0.15	0.77	0.460	0.119	0.010	0.12
2	20	7	2	9.7	9.85	0.2	0.3	9.78	0.25	0.87	0.601	0.141	0.011	0.141
2	21	7	3	9.7	9.85	0.3	0.45	9.78	0.37	0.99	0.358	0.106	0.017	0.107
2	22	7	4	9.7	9.85	0.45	0.65	9.78	0.55	1.17	0.344	0.106	0.008	0.107
2	23	7	5	9.7	9.85	0.65	1.0	9.78	0.81	1.43	0.194	0.091	0.012	0.092
2	24	8	0	9.85	10	0.0	0.2	9.93	0.1	0.68	0.750	0.152	0.060	0.163
2	25	8	1	9.85	10	0.2	0.4	9.93	0.3	0.88	0.573	0.140	0.048	0.148
2	26	8	2	9.85	10	0.4	0.65	9.93	0.52	1.1	0.437	0.136	0.022	0.138

Table 7: Same as Table 5 for Setting 3.

S	idx	E_{idx}	t_{idx}	E_{low} (GeV)	E_{high} (GeV)	Δt_{low} (GeV^2)	Δt_{high} (GeV^2)	E_{avg} (GeV)	Δt_{avg} (GeV^2)	$\lvert t\rvert_{\text{avg}}$ (GeV^2)	$d\sigma/dt$ (nb/GeV^2)	± stat	± sys	± tot
3	0	1	0	8.7	8.9	0.75	1.1	8.8	0.91	1.93	0.156	0.056	0.021	0.06
3	2	2	0	8.9	9.1	1.15	1.55	9.0	1.34	2.24	0.069	0.032	0.011	0.034
3	3	2	1	8.9	9.1	1.55	1.95	9.0	1.74	2.64	0.031	0.031	0.005	0.031
3	4	3	0	9.1	9.25	1.3	1.8	9.18	1.53	2.34	0.053	0.039	0.008	0.04
3	5	3	1	9.1	9.25	1.8	2.35	9.17	2.05	2.87	0.051	0.033	0.005	0.033
3	6	4	0	9.25	9.4	1.6	2.15	9.32	1.85	2.61	0.086	0.039	0.007	0.04
3	7	4	1	9.25	9.4	2.15	2.7	9.33	2.4	3.15	0.064	0.036	0.010	0.037
3	8	5	0	9.4	9.55	1.8	2.3	9.48	2.03	2.73	0.047	0.040	0.006	0.04
3	9	5	1	9.4	9.55	2.3	2.95	9.47	2.58	3.29	0.036	0.025	0.004	0.025
3	10	6	0	9.55	9.7	2.1	2.6	9.62	2.33	2.99	0.089	0.043	0.015	0.045
3	11	6	1	9.55	9.7	2.6	3.25	9.62	2.88	3.54	0.03	0.022	0.003	0.022
3	12	7	0	9.7	9.85	2.3	2.9	9.77	2.56	3.18	0.021	0.029	0.002	0.029
3	13	7	1	9.7	9.85	2.9	3.45	9.77	3.14	3.76	0.025	0.021	0.001	0.021
3	14	8	0	9.85	10	2.5	3.05	9.92	2.75	3.33	0.074	0.048	0.008	0.049
3	15	8	1	9.85	10	3.05	3.7	9.93	3.34	3.92	0.010	0.015	0.001	0.015
3	16	9	0	10	10.15	2.85	3.45	10.08	3.12	3.67	0.014	0.023	0.003	0.023
3	17	9	1	10	10.15	3.45	4.1	10.08	3.74	4.29	0.019	0.016	0.001	0.016
3	19	10	1	10.15	10.3	3.7	4.3	10.23	3.97	4.49	0.002	0.009	0.001	0.009
3	20	11	0	10.3	10.45	3.55	4.0	10.39	3.76	4.25	0.073	0.058	0.017	0.061
3	21	11	1	10.3	10.45	4	4.55	10.38	4.25	4.74	0.027	0.023	0.004	0.024
3	22	12	0	10.45	10.6	3.8	4.4	10.53	4.07	4.54	0.014	0.034	0.003	0.034

Table 8: Same as Table 5 for Setting 4.

S	idx	E_{idx}	t_{idx}	E_{low} (GeV)	E_{high} (GeV)	Δt_{low} (GeV^2)	Δt_{high} (GeV^2)	E_{avg} (GeV)	Δt_{avg} (GeV^2)	$\|t\|_{\text{avg}}$ (GeV^2)	$d\sigma/dt$ (nb/GeV^2)	± stat	± sys	± tot
4	0	3	0	9.1	9.25	0.1	0.25	9.18	0.17	0.98	0.415	0.285	0.042	0.288
4	1	3	1	9.1	9.25	0.25	0.4	9.18	0.32	1.13	0.295	0.210	0.032	0.212
4	2	4	0	9.25	9.4	0.15	0.4	9.33	0.27	1.02	0.403	0.140	0.045	0.147
4	3	4	1	9.25	9.4	0.4	0.65	9.32	0.52	1.28	0.221	0.089	0.013	0.09
4	4	4	2	9.25	9.4	0.65	0.95	9.33	0.79	1.54	0.269	0.100	0.026	0.103
4	5	5	0	9.4	9.55	0.3	0.6	9.48	0.44	1.14	0.417	0.114	0.027	0.117
4	6	5	1	9.4	9.55	0.6	0.9	9.48	0.74	1.44	0.173	0.067	0.020	0.07
4	7	5	2	9.4	9.55	0.9	1.2	9.47	1.04	1.75	0.124	0.071	0.017	0.073
4	8	6	0	9.55	9.7	0.4	0.7	9.63	0.54	1.2	0.389	0.132	0.028	0.135
4	9	6	1	9.55	9.7	0.7	1.1	9.63	0.88	1.54	0.250	0.061	0.010	0.062
4	10	6	0	9.7	9.85	0.65	1.0	9.78	0.81	1.43	0.298	0.087	0.015	0.089
4	12	7	1	9.7	9.85	1	1.35	9.78	1.16	1.78	0.101	0.047	0.005	0.047
4	13	7	2	9.7	9.85	1.35	1.75	9.78	1.53	2.15	0.043	0.041	0.007	0.042
4	14	8	0	9.85	10	0.9	1.4	9.92	1.13	1.71	0.102	0.049	0.016	0.051
4	15	8	1	9.85	10	1.4	2.05	9.92	1.69	2.27	0.106	0.040	0.010	0.041
4	16	9	0	10	10.15	0.95	1.5	10.07	1.2	1.75	0.325	0.086	0.009	0.086
4	17	9	1	10	10.15	1.5	2.2	10.07	1.8	2.35	0.116	0.041	0.014	0.043
4	18	10	0	10.15	10.3	1.2	1.8	10.23	1.47	1.99	0.213	0.074	0.017	0.076
4	19	10	1	10.15	10.3	1.8	2.45	10.23	2.09	2.61	0.097	0.042	0.003	0.042
4	20	11	0	10.3	10.45	1.35	1.95	10.38	1.62	2.11	0.167	0.085	0.005	0.085
4	21	11	1	10.3	10.45	1.95	2.6	10.38	2.24	2.73	0.043	0.034	0.002	0.034
4	22	12	0	10.45	10.6	1.7	2.55	10.55	2.06	2.52	0.060	0.046	0.009	0.046

References

[1] Kiminad A. Mamo and Ismail Zahed. Diffractive photoproduction of J/ψ and Υ using holographic QCD: gravitational form factors and GPD of gluons in the proton. *Phys. Rev. D*, 101(8):086003, 2020.

[2] Kiminad A. Mamo and Ismail Zahed. Nucleon mass radii and distribution: Holographic QCD, Lattice QCD and GlueX data. *Phys. Rev. D*, 103(9):094010, 2021.

[3] Yuxun Guo, Xiangdong Ji, and Yizhuang Liu. QCD Analysis of Near-Threshold Photon-Proton Production of Heavy Quarkonium. *Phys. Rev. D*, 103(9):096010, 2021.

[4] Kiminad A. Mamo and Ismail Zahed. J/ψ near threshold in holographic QCD: A and D gravitational form factors. 4 2022.

[5] Tie-Jiun Hou et al. New CTEQ global analysis of quantum chromodynamics with high-precision data from the LHC. *Phys. Rev. D*, 103(1):014013, 2021.

[6] A. Ali et al. First Measurement of Near-Threshold J/ψ Exclusive Photoproduction off the Proton. *Phys. Rev. Lett.*, 123(7):072001, 2019.

[7] A. V. Belitsky and A. V. Radyushkin. Unraveling hadron structure with generalized parton distributions. *Phys. Rept.*, 418:1–387, 2005.